**J.-C. Grivel**

*Department of Energy Conversion and Storage,*
*Technical University of Denmark,*
*399 Frederiksborgvej, Roskilde, DK-4000, Denmark*
*jean@dtu.dk*

# Subsolidus phase equilibria of the CuO – SrO – ZnO pseudoternary system in air at 900 °C

The subsolidus phase equilibria of the CuO – SrO – ZnO system were determined at 900 °C in air. The pseudoternary section does not contain ternary oxide phases but is made of 5 three-phase regions and 2 narrow two-phase regions linked to a $Sr_{14}Cu_{24-x}Zn_xO_{41-y}$ solid solution. The maximum solubility of Zn in this phase is limited to $x \approx 0.1$, but this low doping level results in a significant decrease of the electrical resistivity by about one order of magnitude compared to the undoped compound. The other binary oxide phases $SrZnO_2$, $Sr_2CuO_3$, and $SrCuO_2$ do not form solid solutions extending into the ternary system. $SrZnO_2$ was found to decompose upon contact with ambient air.

**Keywords:** phase equilibria, isothermal section, oxide systems, pseudoternary, CuO, SrO, ZnO, spin-ladder, electrical resistivity

## Introduction

The discovery of high-temperature superconductivity in the Ba-doped $La_2CuO_4$ insulator [1] has initiated a wealth of research aiming at finding new compounds with ever higher superconducting critical temperatures, in particular among cuprate compounds. One of the strategies used for this purpose consists in studying the phase equilibria of pseudoternary and higher dimensional systems containing CuO and an alkaline earth oxide, in particular BaO, SrO or CaO. Nevertheless, whereas ternary sections involving these oxides with rare-earth oxides have been systematically determined (reference [2] and references therein), combinations of CuO and (BaO, SrO or CaO) with a transition metal oxide are still poorly investi-

gated. In the case of SrO, the exceptions encompass systems in which the transition element is V [3], Nb [4, 5], Fe [6], Ti [7, 8], Zr [8], Hf [8], Ta [9], W [10] and Co [11]. The CuO – SrO – ZnO system does not appear to have been studied. However, Zn being not magnetic, it represents a favorable case for high-temperature superconductors. Furthermore, the use of ZnO in association with SrO or CuO for various applications [12–19] as well as that of $SrZnO_2$ as a catalyst for PET depolymerization under microwave irradiation [20] or as host material for red or blue emitting phosphors [21, 22] make the study of this system interesting in view of optimizing the processing parameters of samples aimed at various technological

applications. The equilibration conditions for the present study (air atmosphere and 900 °C) correspond to conditions similar to those used for the synthesis of various high temperature superconductors [23, 24]. Surprisingly, searches in databases such as the ACerS-NIST Phase Equilibria Diagrams database (version 4.0) or Web of Science did not deliver references to CuO – ZnO or SrO – ZnO pseudobinary systems, not even as side-systems in ternary or higher dimensional systems so that even these simple combinations call for investigations.

## Experimental

CuO (Alfa Aesar, 99.995% purity), $SrCO_3$ (Sigma Aldrich, 99.95) and ZnO (Alfa Aesar, 99.9%) powders were used as starting reagents. 33 different nominal compositions were selected and studied. After the powders were weighted in proper amounts, they were thoroughly mixed in an agate mortar and calcined at 900 °C for 60 h. After this first treatment and further grinding, 1 g pellets with 12 mm diameter were pressed under a pressure of 1.8 kbar and sintered at least twice at 900 °C for 100 h with intermediate grinding and re-pressing. The pellets were quenched in air at the end of each heat treatment. All manipulations were performed in air.

The phase composition of the samples was determined using X-ray diffraction (XRD) patterns recorded in a Bruker D8 Robot diffractometer using Cu Kα radiation (λ = 1.54 Å). Equilibrium was considered as achieved when no differences were detectable in the XRD patterns after two consecutive heat treatments. Si powder was added as an internal standard after the heat treatments for lattice parameter calculations.

Low temperature electrical resistivity measurements were conducted in a Displex setup with a DC current of 1 mA by the 4-contact method on samples cut from the pellets into parallelepipeds with 1.5 × 1.5 mm² cross section and 8 mm length. Gold wires were attached with silver paste cured at 200 °C.

## Results and discussion

As expected, the "ZnO" sample annealed at 900 °C consists of the ZnO (zincite) phase. Its hexagonal lattice parameters were calculated as $a = 3.250(1)$ Å and $c = 5.206(1)$ Å, in close agreement with the values reported by McMurdie et al. [25]. Including small amounts (1 at.%) of either Sr or Cu in the nominal composition resulted in two-phase mixtures, as shown in Fig. 1a, with the appearance of $SrZnO_2$ or CuO peaks, respectively. The lattice parameters of these samples are compared with those of the pure ZnO composition in Table 1. For the $Zn_{0.99}Sr_{0.01}O_2$ nominal composition, the lattice parameters are unchanged within the standard deviation, whereas for $Zn_{0.99}Cu_{0.01}O_2$, a slight decrease of the $c$-axis length seems to take place. The possibility of introducing Sr into the zincite structure has been explored within various contexts such as modification of the optical and electrical properties of ZnO [12, 13], improving its photocatalytic properties [14, 15], or using SrO as a sintering aid [15, 16].

Conclusions on the actual doping of Sr into ZnO are contradictory, probably due to the widely different preparation routes used for these various applications. Güntürkun and Toplan [16] (solid state reaction at 1000 °C to 1300 °C) found

a two-phase equilibrium between ZnO and SrZnO$_2$ even for 1 wt.% SrO in ZnO. Harish et al. [14] (hydrothermal synthesis) reached a similar conclusion. In contrast, Vijaran et al. [13] (thin films made by chemical bath deposition) as well as Srivastava et al. [12] (thin films made by solution spin coating and annealing at 400 °C) claim that Sr enters the ZnO structure. However, the lattice constants of ZnO show a nonmonotonic behavior versus doping level, with the $c$-axis parameter first decreasing before increasing. On the other hand, Das et al. [15] (solid-state reaction at 1100 °C) observed a broadening of some ZnO XRD peaks at low Sr doping level and concluded that two distinct ZnO phases with different lattice constants coexist. Besides the fact that processing condicitons may induce different metastable situations, it is worth mentioning that the relatively low signal-to-noise ratio in the XRD patterns of the thin film samples [12, 13] makes the detection of low intensity impurity peaks difficult, while some high intensity XRD reflections of SrZnO$_2$ have a near overlap with several ZnO reflections. The latter fact may partly be responsible for the reported behavior of the ZnO $c$-axis parameter upon Sr doping [12, 13, 15]. In any case, there is a clear need for more systematic investigations in order to assess the actual solubility of Sr in ZnO and its dependence on processing parameters. The present study allows concluding that for equilibration at 900 °C in air, the solubility of Sr is clearly lower than 1 at.%.

Concerning Cu substitution in ZnO, some recent publications, in which 5 at.% Cu doped samples systematically show a clear CuO XRD impurity peaks [17, 18, 26], claim that a non-negligible amount of Cu actually enters the zincite structure. Again, the very different processing parameters,

including hydrothermal systhesis [17], xerogel route [18] or sol-gel [26], all with relatively brief heat treatments at 600 °C or lower temperatures, certainly have an influence on the conclusions. Moreover, no precise studies based on systematic lattice parameters variation were presented. The results of the present equilibration study at 900 °C are in fact more in line with other studies, including TEM characterization showing that CuO nanoparticles segregate on the surface of ZnO crystallites even for 1 at.% Cu doping [19]. The slight decrease of the ZnO $c$-axis length could be due to very low level Cu doping (ppm range) as observed in ZnO samples exhibiting green luminescence [27].

The presence of CuO in the XRD pattern of the sample with Zn$_{0.99}$Cu$_{0.01}$O$_2$ nominal stoichiometry indicates that there are no binary oxide compounds between ZnO and CuO. This is further confirmed by the fact that ZnO is detected in the XRD pattern of a sample with Zn$_{0.01}$Cu$_{0.99}$O$_2$ overall composition (Fig. 1b). In spite of this two-phase equilibrium, it is clear, as shown in Table 1, that the presence of Zn has resulted in changes in the lattice parameters of CuO, with, in particular, a significant
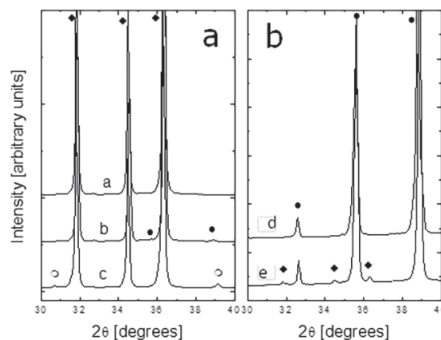


Fig. 1. XRD patterns of samples with ZnO (a), Zn$_{0.99}$Cu$_{0.01}$O$_2$ (b), Zn$_{0.99}$Sr$_{0.01}$O$_2$ (c), CuO$_2$ (d) and Cu$_{0.99}$Zn$_{0.01}$O$_2$ (e) nominal compositions: ◆ – ZnO, ● – CuO, ○ – SrZnO$_2$

decrease of the *b*-axis length and increase of the *a*-axis parameter (as well as an increase of the β-angle from 99.5° to 99.7°). The unambiguous detection of low-intensity ZnO reflections in the XRD pattern of the $Cu_{0.99}Zn_{0.01}O_2$ sample, however, indicates that at 900 °C the solubility limit of Zn into CuO is lower than 1 at. %. Similar lattice parameter variations upon Zn doping in CuO had beed reported previously [28]. Prabhakaran and Boothroyd [29] report up to 5 at. % Zn doping, but the processing conditions in that case (single crystals grown by the floating-zone method under 4 to 8 atm pressure) mostly provide a hint that the solubility limit of Zn in CuO might in-

crease with temperature and may also show some dependence on the oxygen pressure.

In the SrO – ZnO binary oxide side system, $SrZnO_2$ was the only binary oxide phase detected in the XRD patterns. The lattice parameters of samples with $Sr_{0.98}Zn_{1.02}O_2$, $Sr_{1.00}Zn_{1.00}O_2$ and $Sr_{1.02}Zn_{0.98}O_2$ (Table 1) show little variation that is well inside the confidence interval. This observation, coupled with evidence for two-phase equilibria in the two samples with nominal composition deviating from $SrZnO_2$ (Fig. 2), indicates that the latter phase has a very narrow solid-solution range, if any. It is worth mentioning that the formation on SrO in the Sr-rich

Table 1

Phases observed in selected samples after equilibration and crystallographic data for the majority phases. Phases listed between brackets are minority phases. Z = ZnO, C = CuO, SZ = SrZnO$_2$, SOH = Sr(OH)$_2$·H$_2$O, S2C = Sr$_2$CuO$_3$, SC = SrCuO$_2$, S14C = Sr$_{14}$Cu$_{24}$O$_{41-y}$

| Nominal composition | Phases | Space group | a [Å] | b [Å] | c [Å] |
|---|---|---|---|---|---|
| ZnO | Z | P63mc | 3.250(1) | – | 5.206(1) |
| $Zn_{0.99}Cu_{0.01}O$ | Z (C) | *P63mc* | 3.251(1) | – | 5.203(1) |
| $Zn_{0.99}Sr_{0.01}O$ | Z (SZ) | *P63mc* | 3.251(1) | – | 5.206(1) |
| $Sr_{1.00}Zn_{1.00}O_2$ | SZ | *Pnam* | 5.843(9) | 3.339(7) | 11.33(4) |
| $Sr_{0.98}Zn_{1.02}O_2$ | SZ (Z) | *Pnam* | 5.841(9) | 3.340(8) | 11.33(4) |
| $Sr_{1.02}Zn_{0.98}O_2$ | SZ (SOH) | *Pnam* | 5.843(9) | 3.340(7) | 11.33(4) |
| $Sr_{1.00}Zn_{0.98}Cu_{0.02}O_2$ | SZ (Z, S2C) | *Pnam* | 5.843(9) | 3.339(7) | 11.33(4) |
| $Sr_{0.98}Zn_{1.00}Cu_{0.02}O_2$ | SZ (Z, S2C) | *Pnam* | 5.841(9) | 3.339(7) | 11.33(4) |
| CuO | C | C2/c | 4.686(2) | 3.424(1) | 5.129(1) |
| $Cu_{0.99}Zn_{0.01}O$ | C (Z) | *C2/c* | 4.702(1) | 3.410(1) | 5.132(1) |
| $Sr_2CuO_3$ | S2C | *Immm* | 12.70(1) | 3.912(1) | 3.499(1) |
| $Sr_2Cu_{0.95}Zn_{0.05}O_3$ | S2C (SZ, SOH) | *Immm* | 12.71(1) | 3.914(2) | 3.501(1) |
| $SrCuO_2$ | SC | *Cmcm* | 3.572(1) | 16.328(3) | 3.913(2) |
| $SrCu_{0.95}Zn_{0.05}O_2$ | SC (Z, S2C) | *Cmcm* | 3.571(1) | 16.329(2) | 3.912(1) |
| $Sr_{14}Cu_{24}O_{41}$ | S14C | *Cccm* | 11.467(3) | 13.395(7) | 27.649(6) |
| $Sr_{14}Cu_{23.9}Zn_{0.1}O_{41}$ | S14C | *Cccm* | 11.468(4) | 13.396(10) | 27.552(8) |
| $Sr_{14}Cu_{23.75}Zn_{0.25}O_{41}$ | S14C | *Cccm* | 11.475(5) | 13.391(11) | 27.564(14) |
| $Sr_{14}Cu_{23.5}Zn_{0.5}O_{41}$ | S14C (Z, SC) | *Cccm* | 11.467(3) | 13.394(8) | 27.532(7) |
| $Sr_{14}Cu_{23}Zn_1O_{41}$ | S14C (Z, SC) | *Cccm* | 11.469(3) | 13.394(6) | 27.532(5) |

composition is assumed from the detection of $Sr(OH)_2 \cdot H_2O$ [30] in the XRD pattern. This assumption is supported by the fact that a sample with a composition closer to pure SrO ($Sr_{0.99}Zn_{0.01}O$ – not shown), still contained some identifiable SrO reflections. The $Sr(OH)_2 \cdot H_2O$ compound appears to form quickly upon exposure to the atmosphere. The XRD pattern of the $Sr_{1.02}Zn_{0.98}O_2$ sample (Fig. 2b) was recorded within less than 1 hour after quenching from 900 °C. In view of potential applications of $SrZnO_2$, it is also important to note that this compound degrades at a moderate rate when exposed to ambient air. After two weeks, formation of $SrCO_3$ was ascertained in the originally single-phase $SrZnO_2$ sample.

In the CuO – SrO pseudobinary side system, the three binary oxide phases $Sr_2CuO_3$, $SrCuO_2$ and $Sr_{14}Cu_{24}O_{41-y}$ were found as expected [31–36]. Replacing 5 at. % of Cu by Zn in the respective compositions of these compounds resulted in samples with equilibrium between three phases. The lattice parameters of $Sr_2CuO_3$ and $SrCuO_2$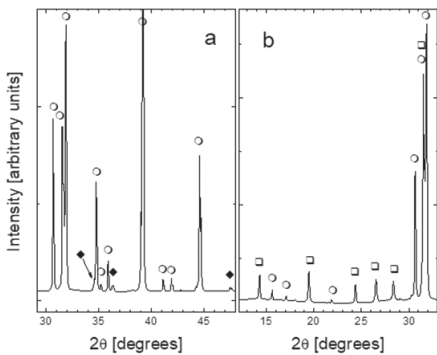 (Table 1) were not affected by the presence of Zn within the confidence interval. In contrast, while the $a$- and $b$-axis lengths of $Sr_{14}Cu_{24}O_{41-y}$ were not influenced, it appears that the $c$-axis lattice parameter became significantly shorter at a Zn substitution level for Cu of 0.4 at. % only. The XRD patterns of samples with $Sr_{14}Cu_{24-x}Zn_xO_{41-y}$ ($x = 0.00$; 0.10; 0.50 and 1.00) nominal compositions are shown in Fig. 3, where it is observed that ZnO and $SrCuO_2$ reflections appear beyond $x = 0.10$ in agreement with the saturation of the $c$-axis parameter value (Table 1 and inset in Fig. 4).

The effect of Zn substitution on the $Sr_{14}Cu_{24}O_{41-y}$ phase was studied further by means of electrical conductivity measurements. As demonstrated by Fig. 4, the room-temperature resistivity of $Sr_{14}Cu_{23.9}Zn_{0.1}O_{41-y}$ is lower than that of $Sr_{14}Cu_{24}O_{41-y}$, the difference increasing at lower temperatures to reach one order of magnitude at 175 K. In the $Sr_{14}Cu_{23.75}Zn_{0.25}O_{41-y}$ sample, the resistivity is even lower. Although the lattice parameters are not changed as compared with the $Sr_{14}Cu_{23.9}Zn_{0.1}O_{41-y}$ composition, it is likely that this further decrease in resistivity is related to a little more Zn doping into the $Sr_{14}Cu_{24}O_{41-y}$ lattice (albeit not all the Zn has entered the structure), instead of being due to minute amounts of impu-
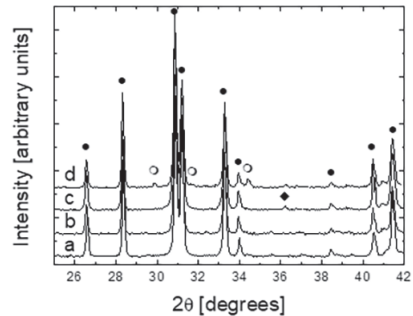


Fig. 2. Details of the XRD patterns of samples with $Sr_{0.98}Zn_{1.02}O_2$ (*a*) and $Sr_{1.02}Zn_{0.98}O_2$ (*b*) nominal compositions showing 2θ ranges, where the appearance of secondary phases is most evident: ◯ – $SrZnO_2$, ◆ – ZnO, ▢ – $Sr(OH)_2 \cdot H_2O$.



Fig. 3. XRD patterns of $Sr_{14}Cu_{24-x}Zn_xO_{41-y}$ samples with $x = 0.00$ (a), 0.10 (b) 0.50 (c) and 0.10 (d): ● – $Sr_{14}Cu_{24}O_{41-y}$, ◯ – $SrCuO_2$, ◆ – ZnO

rity phases. This hypothesis is based on the fact that the samples with higher nominal Zn contents, i.e. $Sr_{14}Cu_{23.5}Zn_{0.5}O_{41-y}$ and $Sr_{14}Cu_{23}Zn_1O_{41-y}$, exhibit higher resistivities (not shown in Fig. 4).

Nominal compositions situated further within the pseudoternary section resulted in two-phase or three-phase equilibria, without any evidence for the formation of ternary oxide phases. Based on all these observations, the phase equilibria and tie-line compatibilities of phases in the CuO – SrO – ZnO system at 900 °C in air can be summarized as shown in Fig. 5. The section contains 5 three-phase regions and 2 narrow two-phase fields associated to the

$Sr_{14}Cu_{24-x}Zn_xO_{41-y}$ solid solution. This system is dominated by ZnO, which is in equilibrium with all other binary oxide phases.

The overall structure of this section is rather different from those of the other systems involving CuO, SrO and a transition element oxide [37–51]. The solubility limit of Co in the $Sr_{14}Cu_{24}O_{41-y}$ structure (up to $Sr_{14}Cu_{19}Co_5O_{41-y}$) is significantly larger than that of Zn. In CuO – SrO – $RE_2O_3$ systems (RE = rare earth element), RE substitution in $Sr_{14}Cu_{24}O_{41-y}$ also takes place to various extents [37–51], however on the Sr sites rather than on the Cu sites, and the pseudoternary sections are dominated by $SrRE_2O_4$ compounds.

## Conclusions

The subsolidus relationship and phase formation of compounds in the CuO – SrO – ZnO system were determined at 900 °C in air. The pseudoternary phase diagram is divided into 5 three-phase fields and two narrow two-phase fields are induced by the narrow $Sr_{14}Cu_{24}Zn_xO_{41-y}$ ($0 \leq x \approx 0.1$) solid solution. Some Zn substitution in CuO can also be inferred from the variation of the lattice parameters of
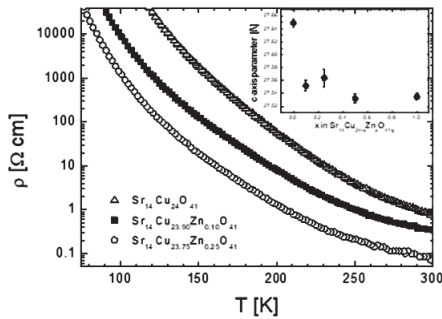
CuO, but the solubility limit of Zn in CuO under the present equilibration conditions is lower than 1 at. %. Substitution of Zn for Cu in the $Sr_{14}Cu_{24}O_{41-y}$ structure has a very strong effect on its electrical resistivity. The fact that ZnO is in equilibrium with all the other phases save SrO represents a favorable situation for processing and testing various properties of ZnO-based multiphase nanoparticles and films.



Fig. 4. Low-temperature electrical resistivity of samples with nominal compositions belonging to the $Sr_{14}Cu_{24-x}Zn_xO_{41-y}$ solid solution. Inset: *c*-axis lattice parameter of the $Sr_{14}Cu_{24}O_{41-y}$ phase in samples with nominal $Sr_{14}Cu_{24-x}Zn_xO_{41-y}$ ($0.0 \leq x \leq 1.0$) compositions


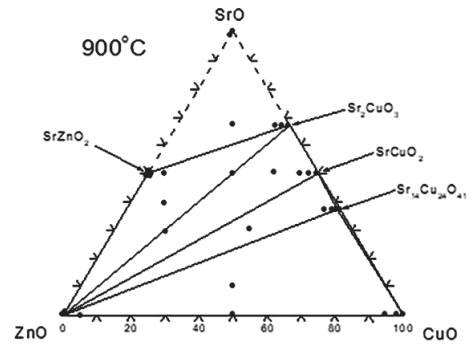
Fig. 5. Phase diagram of the CuO – SrO – ZnO pseudoternary system at 900 °C in air. The studied compositions are marked by symbols. The SrO – $SrZnO_2$ – $Sr_2CuO_3$ area was not studied in details due to the fast reaction of SrO with ambient air

# References

1. Bednorz JG, Muller KA. Possible high-$T_c$ superconductivity in the Ba-La-Cu-O system. *Zeitschrift für Physik.* 1986; B64:189–93. DOI: 10.1007/BF01303701.

2. Grivel JC. Subsolidus phase relations of the CaO – REO$_x$ – CuO systems (RE = Eu, Tb, Dy, Ho, Er, Lu and Sc) at 900 °C in air. *J Phase Equilib Diffus.* 2016;37:601–10. DOI: 10.1007/s11669-016-0489-4.

3. Zhuravlev VD, Velikodnyi YA, Kristallov LV. Study of phase-equilibria in the CuO – SrO – $V_2O_5$ system. *Zh Neorg Khim.* 1987;32:3060–3.

4. Drozdova NM, Sirotinkin VP, Evdokimov AA. Phase correlations in subsolidus domain of SrO – CuO – $Nb_2O_5$ system. *Zh Neorg Khim.* 1991;36:1588–9.

5. Sirotinkin VP, Drozdova NM. Phase relations in SrO – CuO – $Nb_2O_5$ system in the spectrum with high strontium oxide content. *Zh Neorg Khim.* 1993;38:1912–3.

6. Yang LT, Liang JK, Song GB, Chang H, Rao GH. Compounds and phase relations in the SrO – $Fe_2O_3$ – CuO, SrO – $Fe_2O_3$ – $Gd_2O_3$ and $Gd_2O_3$ – $Fe_2O_3$ – CuO ternary systems. *J Alloys Compd.* 2003;353:301–6. DOI: 10.1016/S0925-8388(02)01301-4.

7. Lee SY, Kim HE, Yoo SI. Subsolidus phase relations in the SrO – CuO – $TiO_2$ ternary system at 950 °C in air. *J Alloys Compd.* 2013:556:210–3. DOI: 10.1016/j.jallcom.2012.11.193.

8. Grivel JC. Subsolidus phase relations of the SrO – $MO_2$ – CuO systems (M = Ti, Zr and Hf) at 900 °C in air. *J Alloys Compd.* 2008;464:457–60. DOI: 10.1016/j.jallcom.2007.10.013

9. Grivel JC. Subsolidus phase relations of the SrO – $Ta_2O_5$ – CuO system at 900 °C in air. *J Alloys Compd.* 2009;486:293–8. DOI: 10.1016/j.jallcom.2009.06.133.

10. Grivel JC. Subsolidus phase relations of the SrO – $WO_3$ – CuO system at 800 °C in air. *J Alloys Compd.* 2012;513:304–9. DOI: 10.1016/j.jallcom.2011.09.104.

11. Grivel JC. Subsolidus phase relations of the CoO$_x$ – CuO – SrO system. *J Phase Equilib Diffus.* 2017;38:646–55. DOI: 10.1007/s11669-017-0581-4.

12. Srivastava A, Kumar N, Misra KP, Khare S. Enhancement of band gap of ZnO nanocrystalline films at a faster rate using Sr dopant. *Electron Mater Lett.* 2014;10:703–11. DOI: 10.1007/s13391-014-3131-9.

13. Vijaran TA, Chandramohan R, Varanarasu S, Thirumalai J, Subramanian SP. *J Mater Sci.* 2008;43:1776–82. DOI: 10.1007/s10853-007-2404-1.

14. Harish S, Sabarinathan M, Archana J, Navaneethan M, Nisha KD, Ponnusamy S, Gupta V, Muthamizhchelvan C, Aswal DK, Ikeda H, Hayakawa Y. Synthesis of ZnO/SrO nanocomposites for enhanced photocatalytic activity under visible light irradiation. *Appl Surf Sci.* 2017;418:147–55. DOI: 10.1016/j.apsusc.2017.01.164.

15. Das T, Das BK, Parashar K, Kumar R, Choudhary HK, Anupama AV, Sahoo B, Sahoo PK, Parashar SKS. Effect of Sr-doping on sinterability, morphology, structure, photocatalytic activity and AC conductivity of ZnO ceramics. *J Mater Sci: Mater Electron.* 2017;28:13587–95. DOI: 10.1007/s10854-017-7198-6.

16. Güntürkün K, Toplan Ö. Densification and grain growth of SrO-doped ZnO. *Ceramics – Silikáty.* 2006;50:225–31.

17. Sharma PS, Dutta RK, Pandey AC. Doping dependent room-temperature ferromagnetism and structural properties of dilute magnetic semiconductor ZnO: $Cu^{2+}$ nanorods. *J Magn Magn Mater.* 2009;321:4001–5. DOI: 10.1006/j.jmmm.2009.07.066.

18. Liu HL, Yang JH, Zhang YJ, Wang YX, Wei MB, Wang DD, Zhao LY, Lang JH, Gao M. Ferromagnetism in Cu-doped ZnO nanoparticles at room temperature. *J Mater Sci: Mater Electron.* 2009;20:628–31. DOI: 10.1007/s10854–008–9776–0.

19. Harish S, Archana J, Sabarinathan M, Navaneethan M, Nisha KD, Ponnusamy S, Muthamizhchelvan C, Ikeda H, Aswal DK, Hayakawa Y. Controlled structural and compositional characteristic of visible light active ZnO/CuO photocatalyst for the degradation of organic pollutants. *Appl Surf Sci.* 2017;418:103–12. DOI: 10.1016/j.apsusc.2016.12.082.

20. Geng LL, Han CH, Zhang D. Catalysis investigation of PET depolymerization by $ZnSrO_2$ under microwave irradiation. *Adv Mater.* 2011;239–42:3194–7. DOI: 10.4028/www.scientific.net/AMR.239-242.3194.

21. Yang HK, Lee JH, Hong WT, Jang HI, Moon BK, Jeong JH and Je JY. Preparation and photoluminescence properties of nano-sized $SrZnO_2$: $Sm^{3+}$ phosphor powders obtained by high-energy ball milling. *Ceram Int.* 2015;41:991–4. DOI: 10.1016/j.ceramint.2014.09.019.

22. Manavbasi A, LaCombe JC. A new blue-emitting phosphor, $SrZnO_2$: $Pb^{2+}$, synthesized by the adipic templated gel route. *J Lumin.* 2007;128:129–34. DOI: 10.1016/j.jlumin.2007.06.002.

23. Maeda H, Tanaka Y, Fukutomi M, Asano T, Togano K, Kumakura H, Uehara M, Ikeda S, Ogawa K, Horiuchi S, Matsui Y. New high-$T_c$ superconductors without rare-earth element. *Physica C.* 1988;153–5:602–7. DOI: 10.1016/0921-4534(88)90727-7.

24. Sheng ZZ, Hermann AM, Bulk superconductivity at 120K in the Tl-Ca/Ba-Cu-O system. *Nature.* 1988;332:138–9. DOI: 10.1038/332138a0.

25. McMurdie H, Morris M, Evans E, Paretzkin B, Wong-Ng W, Ettlinger L, Hubbard C. JCPDS reference pattern 36-1451.

26. Modwi A, Lemine OM, Alshammari M, Houas A. Ferromagnetism at room temperature in $Zn_{0.95}Cu_{0.05}O$ nanoparticles synthesized by sol-gel method. *Mater Lett.* 2017;194:98–101. DOI: 10.1016/j.matlet.2017.02.029.

27. Garces NY, Wang L, Bai L, Giles NC, Halliburton LE, Cantwell G. Role of copper in the green luminescence from ZnO crystals. *Appl Phys Lett.* 2002;81:622–4. DOI: 10.1063/1.1494125

28. Borzi RA, Stewart SJ, Punte G, Mercader RC, Zysler RD, Tovar M. History-dependent magnetic properties in pure and Zn-doped cupric oxide. *Solid State Commun.* 2001;117:311–4. DOI: 10.1016/S0038-1098(00)00467-1.

29. Prabhakaran D, Boothroyd AT. Single crystal growth of Zn-doped CuO by the floating-zone method. *J Cryst Growth.* 2003;250:77–82. DOI: 10.1016/S0022-0248(02)02230-3.

30. Buchmeier W, Lutz HD. Crystal-structures of $Sr(OH)_2 \cdot H_2O$, $Ba(OH)_2 \cdot H_2O$ (O-RH and MON) and $Ba(OH)_{2.3} \cdot H_2O$. *Z Anorg Allg Chem.* 1986;538:131–42. DOI: 10.1002/zaac.19865380713.

31. Liang JK, Zhan C, Fei W, Xie SS. Phase-diagram of SrO – CaO – CuO ternary-system. *Solid State Commun.* 1990;75:247–52. DOI: 10.1016/0038-1098(90)90279-K

32. Kosmynin AS, Slobodin BV, Balashov VL, Garkushin IK, Fotiev AA, Trunin AS. Phase-equilibria in the CaO-SrO-CuO system (≥ 70 mol% CuO). *Inorg Mater.* 1995;7:867–70.

33. Hwang NM, Roth RS, Rawn CJ. Phase-equilibria in the systems SrO-CuO and SrO-1/2Bi$_2$O$_3$. *J Am Ceram Soc.* 1990;73:2531–3. DOI: 10.1111/j.1151-2916.1990.tb07628.x.

34. Suzuki RO, Bohac P, Gauckler LJ. Thermodynamics and phase-equilibria in the Sr-Cu-O system. *J Am Ceram Soc.* 1992;75:2833–42. DOI: 10.1111/j.1151-2916.1992.tb05513.x.

35. Nevřiva M, Kraus H. Study of phase-equilibria in the partially open Sr-Cu-(O) system. *Physica C.* 1994;235–40:325–6. DOI: 10.1016/0921-4534(94)91386–2.

36. Alcock CB, Li BZ. Thermodynamic study of the Cu-Sr-O system. *J Am Ceram Soc.* 1990;73:1176–80. DOI: 10.1111/j.1151–2916.1990.tb05176.x.

37. De Leeuw DM, Mutsaers CAHA, Geelen GPJ, Smoorenburg HCA, Langereis C. Compounds and phase compatibilities in the system Y$_2$O$_3$ – (BaO) – SrO – CuO at 950 °C. *Physica C.* 1988;152:508–12. DOI: 10.1016/0921-4534(88)90061-5.

38. Wu F, Xie S, Chen Z, Ling JK. Subsolidus phase-relations of the Y$_2$O$_3$ – SrO – CuO system. *J Mater Sci.* 1992;27:3082–4. DOI: 10.1007/BF01154122.

39. Roth RS, Rawn CJ, Whitler JD, Chiang CK, Wong-Ng W. Phase-equilibria and crystal-chemistry in the quaternary system Ba-Sr-Y-Cu-O in air. *J Am Ceram Soc.* 1989;72:395–9. DOI: 10.1111/j.1151-2916.1989.tb06142.x.

40. De Leeuw DM, Mutsaers CAHA, Geelen GPJ, Langereis C. Compounds and phase compatibilities in the system La$_2$O$_3$ – SrO – CuO at 950 °C. *J Solid State Chem.* 1989;80:276–85. DOI: 10.1016/0022-4596(89)90090-X.

41. Chen X, Liang JK, Wang C, Rao GH, Xing XR, Song ZH, Qiao ZY. The Nd$_2$O$_3$ – SrO – CuO system – compounds and phase-relations. *J Alloys Compd.* 1994;205:101–6. DOI: 10.1016/0925-8388(94)90773-0.

42. Han CQ, Chen XL, Liang JK, Liu QL, Rao GH. The ternary system Sm$_2$O$_3$ – SrO – CuO: compounds and phase relations. *J Alloys Compd.* 200;314:301–4. DOI: 10.1016/S0925-8388(00)01255-X.

43. Han CQ, Chen XL, Liang JK, Liu QL, Rao GH. The ternary system Eu$_2$O$_3$ – SrO – CuO: compounds and phase relations. *J Solid State Chem.* 2001;156:247–50. DOI: 10.1006/jssc.2000.8997.

44. Han CQ, Gao Y, Chen XL, Liang JK, Rao H. The ternary system Gd$_2$O$_3$ – SrO – CuO: compounds and phase relations. *J Alloys Compd.* 2001;321:54–9. DOI: 10.1016/S0925-8388(01)00873-8.

45. Wong-Ng W, Huang Q, Levin I, Kaduk JA, Dillingham J, Haugan T, Suh J, Cook LP. Crystal chemistry and phase equilibria of selected SrO – R$_2$O$_3$ – CuO$_x$ and related systems; R = lanthanides and yttrium. *Int J Inorg Mater.* 2001;3:1283–90. DOI: 10.1016/S1466-6049(01)00133-7.

46. Wong-Ng W, Dillingham J, Cook LP. Phase relations of the SrO – Ho$_2$O$_3$ – CuO$_x$ system. *J Solid State Chem.* 2000;149:333–7. DOI: 10.1006/jssc.1999.8536.

47. Grivel JC, Andersen NH. Subsolidus phase relations of the SrO – $Er_2O_3$ – CuO system. *J Alloys Compd.* 2005;389:186–9. DOI: 10.1016/j.jallcom.2004.05.086.

48. Han CQ, Chen XL, Liang JK, Liu QL, Chen Y, Rao GH. The ternary system $Tm_2O_3$ – SrO – CuO: compounds and phase relations. *J Alloys Compd.* 2000;309:95–9. DOI: 10.1016/S0925–8388(00)01041–0.

49. Dillingham J, Wong-Ng W, Levin I. Phase equilibria of the SrO – $Yb_2O_3$ – $CuO_x$ system in air. *Int J Inorg Mater.* 2001;3:569–73. DOI: 10.1016/S1466-6049(01)00015-0.

50. Grivel JC, Andersen NH. Subsolidus phase relations of the SrO – $RE_2O_3$ – CuO systems (RE = Tm, Lu and Sc). *J Alloys Compd.* 2005;391:292–5. DOI: 10.1016/j.jallcom.2004.08.077.

51. Grivel JC, Andersen NH. Subsolidus phase relations of the SrO – $REO_x$ – CuO systems (RE = Ce, Pr and Tb). *J Alloys Compd.* 2007;436:261–5. DOI: 10.1016/j.jallcom.2006.07.020.